Implementation of LDA+DMFT with the pseudo-potential-plane-wave method*

Zhao Jian-Zhou(赵建洲)[a)b)], Zhuang Jia-Ning(庄嘉宁)[a)], Deng Xiao-Yu(邓小宇)[a)c)], Bi Yan(毕 延)[b)], Cai Ling-Cang(蔡灵仓)[b)], Fang Zhong(方 忠)[a)], and Dai Xi(戴 希)[a)†]

[a)] *Institute of Physics, Chinese Academy of Sciences, Beijing* 100190, *China*

[b)] *National key Laboratory of Shock Wave and Detonation Physics, Institute of Fluid Physics, China Academy of Engineering Physics, Mianyang* 621900, *China*

[c)] *Centre de Physicque Théorique, Ecole Polytechnique, CNRS,* 91128 *Palaiseau Cedex, France*

(Received 26 December 2011; revised manuscript received 30 January 2012)

We propose an efficient implementation of combining dynamical mean field theory (DMFT) with electronic structural calculation based on the local density approximation (LDA). The pseudo-potential-plane-wave method is used in the LDA part, which enables it to be applied to large systems. The full loop self consistency of the charge density has been reached in our implementation, which allows us to compute the total energy related properties. The procedure of LDA+DMFT is introduced in detail with a complete flow chart. We have also applied our code to study the electronic structure of several typical strong correlated materials, including cerium, americium and NiO. Our results fit quite well with both the experimental data and previous studies.

Keywords: LDA+DMFT, strong correlated electrons

PACS: 71.27.+a, 71.15.Mb, 71.15.Nc, 71.20.–b **DOI:** 10.1088/1674-1056/21/5/057106

1. Introduction

The first principles calculation based on the density functional theory (DFT) with the local density approximation (LDA) and its generalization generalized gradient approximation (GGA) is very successful in predicting ground-state properties and band structures of a wide range of real materials.[1−4] However, it has been known for a long time that it is not sufficient for calculating the electronic structure of strongly correlated materials (i.e., transition metal oxides, actinide and lanthanide-based materials, and high T_c superconductors) by these methods alone, even on a qualitative level. In order to overcome these shortcomings of the traditional DFT–LDA scheme, remedies such as LDA+U have been proposed, which can describe some of the strong correlated materials with long-range order in their ground states. However, even LDA+U cannot be applied to many of the strongly correlated materials, such as the paramagnetic Mott insulator phase and the materials containing an unfilled f-shell with strong multiplet effects.

Therefore, it is important to have a first principles method which can be applied to the strongly correlated materials with the ability to capture the dynamical properties, finite temperature properties and multiplet effects. In the last two decades, the dynamical mean field theory (DMFT) has been developed very quickly to be the standard tool to deal with the on-site correlation effect in the limit of large dimensions.[5] After being successfully applied to many model systems, DMFT has been considered as a powerful tool to capture the on-site correlation effects based on the Hubbard-like Hamiltonians containing both the local interaction terms and the single-particle Hamiltonians extracted from LDA. Thus, the LDA+DMFT method, which combines the DFT-based band structure techniques with DMFT, has been proposed and developed quickly in the last decade. By DMFT, the local correlation effect can be well described by the self energy, which has frequency dependence and in general takes the matrix form within the subspace spanned by the correlation orbitals. Using the Green's function containing self energy, many physical properties of strongly correlated materials can be calculated, such

*Project supported by the National Basic Research Program of China (Grant No. 2011CBA00108), the National Natural Science Foundation of China (Grants Nos. 10876042 and 10874158), the Development Foundation of China Academy of Engineering Physics (Grants Nos. 2008A0101001 and 2010A0101001), and the Fund of the Laboratory of Shock Wave and Detonation Physics, Institute of Fluid Physics, China Academy of Engineering Physics (Grant No. 2011-056000-0833F).

†Corresponding author. E-mail: daix@aphy.iphy.ac.cn

© 2012 Chinese Physical Society and IOP Publishing Ltd

as the electronic spectral function, the total energy, the optical conductivity, and the local spin susceptibility.

Most of the LDA+DMFT calculations till now have been performed by the partially self-consistent scheme, where the local self-energy is obtained by the DMFT calculation with a fixed LDA Hamiltonian generated from the fixed LDA charge density. Therefore, in this simplified scheme, one neglects the inference of the strong on-site Coulomb interaction on the charge density. The above-mentioned "one-shot" DMFT calculation works quite well for the electronic structure. While in order to obtain reliable total energy related properties, i.e., the equilibrium volume, the elastic constants and the phonon frequencies, an LDA+DMFT scheme with full charge density self consistency is needed. Up to date, there have been several fully self-consistent LDA+DMFT schemes[6,7] as well as actual implementations.[8−11] As mentioned in Ref. [11], there are three major issues that have to be addressed in DFT+DMFT implementations: 1) quality of the basis set; 2) quality of the impurity solvers; 3) choice of correlated orbitals onto which the full Green's function is projected. In the implementations of LDA+DMFT mentioned above with full charge self-consistency, the basis set of the linear muffin-tin orbitals (LMTO) are used, and the local correlated orbitals are naturally chosen based on the muffin-tin orbitals. However, there are very few implementations of LDA+DMFT with full charge self-consistency based on the plane-wave methods.

In the present paper, we implement a full self-consistent LDA+DMFT scheme using pseudo-potential-plane-wave as the basis set, and we use either atomic orbitals or Wannier orbitals depending on different physics systems. The Hubbard-I approximation is used as the impurity solver in the present paper, but it can be replaced by a more precise solver like the continuous-time quantum Monte Carlo (CTQMC) method for metallic systems. The present paper is organized as follows: in Section 2, we describe how to choose and construct the correlated orbitals onto which the local interactions exert. In Section 3, we show the full-loop flow and LDA+DMFT (Hubbard-I) formalism in detail. We apply this LDA+DMFT approach to several correlated materials such as Ce, Am, and NiO in Section 4. Finally we conclude our work in Section 5.

2. Projection onto localized orbitals

In the LDA+DMFT calculation, all the energy bands are divided into two groups. And only the on-site interactions among those local orbitals are treated more precisely by DMFT. Therefore, the choice of localized orbitals affects the results obtained by using the LDA+DMFT method and becomes one of the important issues in LDA+DMFT. A natural choice for the local orbitals is a set of atomic-like wave functions with the corresponding d or f characters. Typical atomic-like local orbitals are the linear muffin-tin orbitals (LMTOs)[12] adopted in early LDA+DMFT implementations.[13−15] However, a more physical choice should be Wannier functions, since the shape of the local orbitals will be altered in crystals especially when there is strong hybridization between localized orbital and delocalized p-type or s-type orbitals. The Wannier functions are not uniquely determined by the Bloch wave functions, so a different choice can be made, such as the Nth-order muffin-tin orbitals,[16] the projected Wannier functions,[17] and the maximally localized Wannier functions (MLWFs).[18,19] Comparisons of these choices have been made in previous literature. In this paper, two kinds of local orbitals, atomic-like functions and the projected wannier functions are adopted according to the different systems.

The implementation of the LDA+DMFT method reported in this paper is developed on an existing DFT package BSTATE (Beijing Simulation Tool of Atomic TEchnique), which is based on pseudo-potentials and plane waves. Unlike the LMTO methods, the local orbitals do not enter the basis set of plane waves and should be constructed in a suitable way. Projected Wannier functions or MLWFs as local orbitals have been used by previously reported LDA+DMFT implementations based on pseudo-potentials (or projector augmented wave (PAW)) method) and the plane-wave scheme.[20−22] In this report, two kinds of orbitals are used according to the need: one is directly derived from the atomic wave function of an isolated atom and the other is projected Wannier functions constructed from these atomic wave functions. In order to be self-contained, the construction procedure is presented below in detail. Since all our calculations are based on a plane-wave set, the local orbitals will be projected onto these plane waves.

First we consider the atomic-like local orbitals. The localized nature of the correlated bands with d or f characters in crystals ensures that these local orbitals

are very similar to the corresponding atomic wave functions of an isolated atom. The atomic wave functions can be picked as the local orbitals directly if the hybridization in crystal could be neglected. All atomic wave functions for the isolated atom could be obtained by solving the all-electron radical Schrödinger equation

$$(T + V(r))\psi_{nl}^{\mathrm{ALL}}(r) = E_{nl}\psi_{nl}^{\mathrm{ALL}}(r). \tag{1}$$

In this manner, all orbitals are well defined by the primer quantum number n and angular quantum number l. In realistic systems, the local orbitals usually come from the partially filled d or f shell and could be picked according to its character. Often there is only one type of local orbital, so the local subspace can be labeled by l. Of course, considering the spherical symmetry of the isolated atom, the spherical harmonics should be multiplied the radical wave functions to form a complete set. The local orbitals are

$$|\phi_{lm,I}\rangle = |\psi_{l,I}^{\mathrm{ALL}}Y_{lm}\rangle, \tag{2}$$

where $m = 1, \ldots, 2l+1$ denote different angular components.

In methods based on plane waves, it is not desirable to use the all-electron wave function directly since it requires a large amount of plane waves to expand in momentum space. To avoid this problem, in PAW method all-electron atomic partial waves can be used, while in pseudo-potentials method, pseudo atomic wave functions can be chosen. The latter is used in this paper. During the generation of pseudo-potentials, the Schrödinger equation obeyed by the pseudo wave functions is

$$(T + V^{\mathrm{PS}}(r))\psi_{nl}^{\mathrm{PS}}(r) = E_{nl}^{\mathrm{PS}}\psi_{nl}^{\mathrm{PS}}(r). \tag{3}$$

Details of the generation of pseudo-potentials can be found in the previous literature.[23,24] The concept of pseudo-potentials is quite straight forward. Beyond a core radius r_{c}, the pseudo-potential V^{PS} plays the role of a scattering center just as a real atomic potential V^{ALL} does. Thus, the pseudo eigen energy E_{nl}^{PS} should be the same as the realistic one E_{nl}^{ALL}, and both the pseudo wave functions $|\psi_{n,I}^{\mathrm{PS}}\rangle$ and the pseudo-potential V^{PS} coincide with the exact wave functions $|\psi_{n,I}^{\mathrm{ALL}}\rangle$ and the realistic potential V^{ALL} of an isolated atoms beyond this core radius r_{c}, respectively.

$$E_{nl}^{\mathrm{PS}} = E_{nl}; \tag{4}$$

$$V^{\mathrm{PS}}(r) = V(r),\ \psi^{\mathrm{PS}}(r) = \psi^{\mathrm{ALL}}(r),\ r > r_{\mathrm{c}}. \tag{5}$$

The quality of pseudo wave functions is the same as the quality of the pseudo-potentials, which could be justified by comparing simple DFT calculations with accepted results. The pseudo wave functions bear the same atomic features as the exact atomic wave functions, and can be picked as the above local orbitals (the angular quantum number l is ignored since usually only one kind of local orbital is considered)

$$|\phi_{m,I}\rangle = |\psi_{l,I}^{\mathrm{PS}}Y_{lm}\rangle. \tag{6}$$

It is convenient to transform the local orbitals from real space to momentum space in crystal calculations

$$|\phi_{m,\boldsymbol{k}}\rangle = \sum_I \mathrm{e}^{\mathrm{i}\boldsymbol{k}\cdot\boldsymbol{R}_I}|\phi_{m,I}\rangle. \tag{7}$$

Since the atomic wave functions at different sites I are not orthogonal, an orthogonalization procedure is needed for the above local orbitals.

The DFT calculations give a set of Bloch waves $|\Psi_{n\boldsymbol{k}}\rangle$ spanning the total Hilbert space in which lies the local subspace spanning by the local orbitals. Thus, the physical choice of local orbitals is Wannier functions derived from the Bloch waves. The Wannier functions are localized in real space and can be constructed from the Bloch waves via a unitary transformation. However, this unitary transformation is not unique since the phase factors of Bloch waves are uncertain, which results in that there are many kinds of Wannier functions in use, e.g., the projected Wannier functions, NMTOs and MLWFs. In addition, it is not necessary to include all the Bloch waves but the relevant bands lying in a certain energy range to construct the Wannier functions. The local orbitals could be picked as a subset of these Wannier functions with specified d or f localized character.

The projecting Wannier functions method is a simple way to construct Wannier functions, in which trial wave functions are projected onto physical relevant Bloch bands. The atomic-like local orbitals mentioned above are used as trial functions here. The Bloch bands can be selected by band indices $(N_i, \ldots, N_j)$ or by an energy interval (E_i, E_j) enclosing them.

$$\begin{aligned} |W_{m,\boldsymbol{k}}\rangle &= \sum_{n=N_i}^{N_j} |\psi_{n\boldsymbol{k}}\rangle\langle\psi_{n\boldsymbol{k}}|\phi_{lm,\boldsymbol{k}}\rangle \\ &= \sum_{n(E_i<\epsilon_{n\boldsymbol{k}}<E_j)} |\psi_{n\boldsymbol{k}}\rangle\langle\psi_{n\boldsymbol{k}}|\phi_{m,\boldsymbol{k}}\rangle. \end{aligned} \tag{8}$$

These orbitals need normalization and orthogonalization to be true Wannier functions

$$|\tilde{W}_{m,\boldsymbol{k}}\rangle = \sum_{m'} O_{m,m'}(\boldsymbol{k})^{-1/2}|W_{m,\boldsymbol{k}}\rangle, \tag{9}$$

where O is the overlap matrix between different $|W_{m,\boldsymbol{k}}\rangle$s

$$O_{m,m'}(\boldsymbol{k}) = \langle W_{m,\boldsymbol{k}}|W_{m',\boldsymbol{k}}\rangle. \tag{10}$$

Although the construction method cannot give the most localized Wannier orbitals, the basic features of the localized bands are captured to a very good extent, as indicated by a few reports,[17,20−22] and also proved by our calculations in this paper.

3. LDA+DMFT (Hubbard-I) formalism

We will introduce the detail procedge of LDA+DMFT with full loop charge density self consistency in this section. First we plot the general flow chart in Fig. 1, which contains an inner DMFT loop and an outer charge density loop. However, if we use Hubbard-I approximation as the impurity solver, the inner DMFT loop is thus neglected.

In the following subsections, we describe the whole process in detail.

3.1. First LDA calculation

The first step of the full loop LDA+DMFT is an LDA self-consistent calculation, whose main purpose is to generate an effective single particle Hamiltonian $\hat{H}_{\mathrm{LDA}}$ and construct the correlated orbitals.

Generally, the effective LDA Hamiltonian can be expressed as follows:

$$\hat{H}_{\mathrm{LDA}} = \sum_{n\boldsymbol{k}} E_{n\boldsymbol{k}} \hat{c}^{\dagger}_{n\boldsymbol{k}} \hat{c}_{n\boldsymbol{k}}. \tag{11}$$

In the above equation, $n = 1, 2, \ldots, N_{\mathrm{band}}$ are the joint indices of band and spin; $E_{n\boldsymbol{k}}$ is the eigen energy of the Kohn–Sham equation determined by $\hat{H}_{\mathrm{LDA}}|\varphi_{n\boldsymbol{k}}\rangle = E_{n\boldsymbol{k}}|\varphi_{n\boldsymbol{k}}\rangle$, where $|\varphi_{n\boldsymbol{k}}\rangle$ represents a set of orthonormal Bloch functions.

The LDA calculation also complements the construction of local correlated orbitals. In the present implementation, the atomic orbitals and the Wannier functions are two types of commonly used local basis. In LDA+DMFT, the local interactions have been considered on the DMFT level only within the local orbitals. To set up the DMFT self-consistent equation, we need to obtain the overlap matrix between local orbitals and Bloch wave functions, which takes the form of $S^{\boldsymbol{k}}_{\alpha,n} = \langle \alpha_{\boldsymbol{k}}|\varphi_{n\boldsymbol{k}}\rangle$, with Greek letter α denoting the index of local orbitals. The completeness of the Bloch basis set gives

$$\sum_{n} |S^{\boldsymbol{k}}_{\alpha,n}|^2 = 1 \tag{12}$$

for any local orbital α and any $\boldsymbol{k}$-point.

3.2. DMFT Loop

The purpose of the DMFT loop is to calculate the self-energy caused by the local interactions through the DMFT self consistent loop. As mentioned above, the DMFT loop is not necessary if we use Hubbard-I approximation as the impurity solver. However, here we first introduce the algorithm with more general impurity solvers.

By adding the local interaction terms to LDA, we obtain the total Hamiltonian of the system which is to be solved by DMFT as

$$\hat{H}_{\mathrm{LDA+DMFT}} = \hat{H}_{\mathrm{LDA}} + \sum_{i} (\hat{H}^{i}_{U} - \hat{V}^{i}_{\mathrm{DC}}) - \mu\hat{N}, \tag{13}$$

where i is the site index. For a specified site, we remove the i index and

$$\hat{H}_{U} = \frac{1}{2} \sum_{\alpha\beta\gamma\delta} U_{\alpha\beta\gamma\delta} \hat{f}^{\dagger}_{\alpha} \hat{f}^{\dagger}_{\beta} \hat{f}_{\gamma} \hat{f}_{\delta} \tag{14}$$

is written as a general form of two-body local interactions, in which the creation and annihilation operators of correlated orbitals $\hat{f}^{\dagger}_{\alpha}$ and $\hat{f}_{\alpha}$ are associated with Bloch operators in term of

$$\hat{f}^{\dagger}_{\alpha} = \sum_{n\boldsymbol{k}} \hat{c}^{\dagger}_{n\boldsymbol{k}} \langle \varphi_{n\boldsymbol{k}}|\alpha_{\boldsymbol{k}}\rangle, \tag{15}$$

$$\hat{f}_{\alpha} = \sum_{n\boldsymbol{k}} \hat{c}_{n\boldsymbol{k}} \langle \alpha_{\boldsymbol{k}}|\varphi_{n\boldsymbol{k}}\rangle. \tag{16}$$

The third term of Eq. (13) is the double-counting term corresponding to the correlated energy that has already been considered in the LDA calculation at a Hartree–Fock mean field level

$$\hat{V}_{\mathrm{DC}} = \sum_{\alpha} V^{\alpha}_{\mathrm{DC}} \hat{f}^{\dagger}_{\alpha} \hat{f}_{\alpha}, \tag{17}$$

and this term will be discussed in Subsection 3.2.3. The last term of Eq. (13)

$$\hat{N} = \sum_{n\boldsymbol{k}} \hat{c}^{\dagger}_{n\boldsymbol{k}} \hat{c}_{n\boldsymbol{k}} \tag{18}$$

is the total number of particle operator, while the chemical potential μ controls the occupation number of the unit cell.

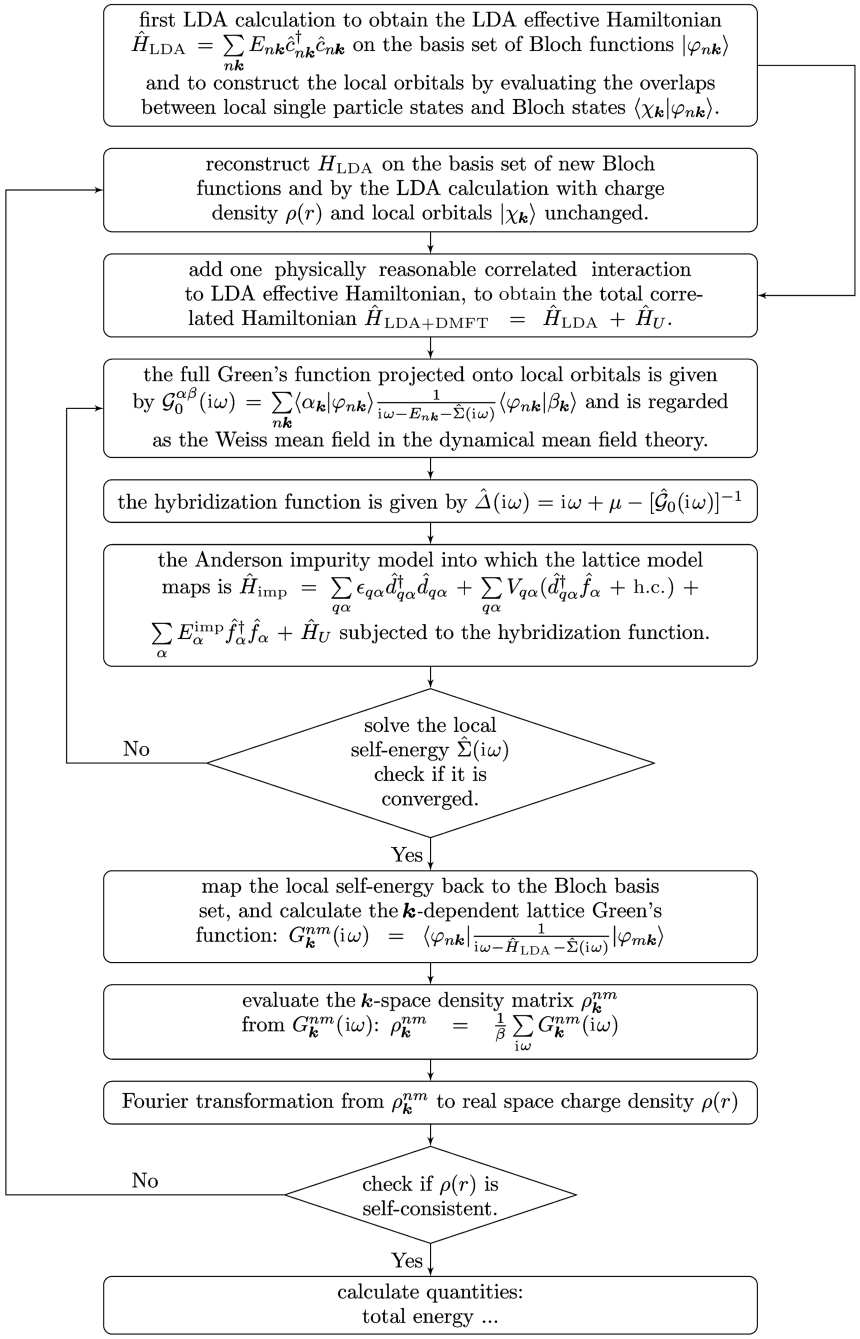


Fig. 1. The most general flow chart for LDA+DMFT scheme. The first LDA calculation gives the band structure on LDA level, and constructs local orbitals. Then the full Hamiltonian is established and solved by a DMFT loop, after which the charge density can be recalculated by Fourier transforming the $\boldsymbol{k}$-space density matrix to real space. The "non-interacting" Hamiltonian is thus regenerated based on the new charge density profile and the calculation will be completed when the self consistency has been reached for the full loop.

3.2.1. Quantum impurity hamiltonian

In DMFT, the correlation problem on the lattice can be mapped to a quantum impurity model, which contains the same on-site interaction and reads

$$\hat{H}_{\rm imp} = \sum_{q\alpha} \epsilon_{q\alpha} \hat{c}^{\dagger}_{q\alpha} \hat{c}_{q\alpha} + \sum_{q\alpha} V_{q\alpha} (\hat{c}^{\dagger}_{q\alpha} \hat{f}_{\alpha} + \mathrm{h.c.}) + \sum_{\alpha} E^{\rm imp}_{\alpha} \hat{f}^{\dagger}_{\alpha} \hat{f}_{\alpha} + \hat{H}_U. \quad (19)$$

The inference from the rest of the lattice site besides the one considered in the impurity model is simulated by a non-interacting "heat bath", which is described by the first term in Eq. (19). The second term describes the coupling between the impurity site and the

heat bath and the rest two terms describe the local interactions.

3.2.2. Hybridization function and Weiss field

The above quantum impurity model can be solved by the impurity solver, i.e., Hubbard-I, and the self energy $\hat{\Sigma}(\mathrm{i}\omega)$ is then obtained, with which we can construct the lattice Green's function by applying the same self energy term as

$$[\hat{G}^{\boldsymbol{k}}_{\mathrm{lattice}}]^{-1} = \mathrm{i}\omega - \hat{H}_{\boldsymbol{k}} - \hat{\Sigma}_{\boldsymbol{k}}(\mathrm{i}\omega) + \mu. \tag{20}$$

The hybridization function, which characterizes the dynamics of the "heat bath", is defined as $\Delta(\mathrm{i}\omega)_{\alpha\beta} = \delta_{\alpha\beta}\sum_q |V_{q\alpha}|^2/(\mathrm{i}\omega - \epsilon_{q\alpha})$ and can be obtained iteratively by the following DMFT self consistent equation:

$$\hat{\Delta}(\mathrm{i}\omega) = \mathrm{i}\omega - \hat{E}_{\mathrm{imp}} - \hat{\Sigma} + \mu - \left[\sum_{\boldsymbol{k}} G^{\boldsymbol{k}}_{\mathrm{lattice}}(\mathrm{i}\omega)\right]^{-1}. \tag{21}$$

The above equation is obtained by requiring that the local Green's function on the lattice should be equal to the Green's function of the quantum impurity problem. Equations (20) and (21) form a closed self-consistent loop, which determines both the self energy and the hybridization function iteratively.

3.2.3. Double counting term

In this section, we discuss the explicit expression of $E^{\mathrm{imp}}_{\alpha}$ as well as the double-counting term in Eq. (13). For 3d system under cubic symmetry, the local interaction can be simplified as Coulomb interaction U and Hund's rule coupling J, which can be written as

$$\begin{aligned}\hat{H}_U =\ & U\sum_b \hat{n}_{b,\uparrow}\hat{n}_{b,\downarrow} + (U-2J)\sum_{\substack{b<b'\\ \sigma\sigma}} \hat{n}_{b,\sigma}\hat{n}_{b',\sigma} \\ & - J\sum_{\substack{b<b'\\ \sigma}} \hat{n}_{b\sigma}\hat{n}_{b'\sigma}.\end{aligned} \tag{22}$$

And the double counting energy in this case has been studied by Held *et al.*,[25] which can be approximately chosen as

$$E_{\mathrm{DC}} = \frac{1}{2}\bar{U} n_{\mathrm{LDA+DMFT}}(n_{\mathrm{LDA+DMFT}} - 1), \tag{23}$$

where

$$\bar{U} = \frac{U + 2(M-1)(U-2J) - (M-1)J}{2M-1}, \tag{24}$$

$$M = 2l + 1, \tag{25}$$

and $n_{\mathrm{LDA+DMFT}}$ is the total number of electrons on correlated orbitals for a specific atom. Hence, Equation (11) becomes

$$\begin{aligned}\hat{V}_{\mathrm{DC}} &= \sum_{\alpha} \frac{\partial E_{\mathrm{DC}}}{\partial n_\alpha}\hat{n}_\alpha \\ &= \sum_{\alpha} \bar{U}\left(n_{\mathrm{LDA+DMFT}} - \frac{1}{2}\right)\hat{n}_\alpha.\end{aligned} \tag{26}$$

The final expression of E^{imp} is

$$E^{\mathrm{imp}}_{\alpha} = \sum_{\boldsymbol{k}} \langle\alpha_{\boldsymbol{k}}|\hat{H}_{\mathrm{LDA}}|\alpha_{\boldsymbol{k}}\rangle - V^{\alpha}_{\mathrm{DC}}, \tag{27}$$

where

$$V^{\alpha}_{\mathrm{DC}} = \bar{U}\left(n_{\mathrm{LDA+DMFT}} - \frac{1}{2}\right). \tag{28}$$

The way to remove the form of double-counting energy is not unique, and in fact this process requires some intuition. The double-counting discussed in the above sections is a very usual way, which is also used in LDA+U method. In addition, the following two ways are also commonly used:

1) to remove self-energy at zero-frequency $\hat{\Sigma}(\mathrm{i}\omega) \to \hat{\Sigma}(\mathrm{i}\omega) - \hat{\Sigma}(0)$,

2) to remove self-energy at infinity-frequency $\hat{\Sigma}(\mathrm{i}\omega) \to \hat{\Sigma}(\mathrm{i}\omega) - \hat{\Sigma}(\infty)$.

Furthermore, the double-counting energy is also regarded as "impurity solver dependent". For example, it is reasonable to use an integer to replace $n_{\mathrm{LDA+DMFT}}$ in Eq. (23) for the Hubbard-I solver,[10] and in this paper we also follow their suggestion.

3.2.4. Hubbard-I solver

The essential point of the Hubbard-I solver is to neglect the effect of the heat bath and take the atomic self energy as the zeroth order approximation for the quantum impurity problem, which can be written as

$$\hat{\Sigma}^{\mathrm{atom}} = [\mathrm{i}\omega_n + \mu_{\mathrm{atom}} - \hat{E}^{\mathrm{imp}}]^{-1} - [\hat{G}^{\mathrm{atom}}]^{-1}, \tag{29}$$

where $\hat{G}^{\mathrm{atom}}$ is the Green's function for a single atom, which can be expressed as

$$\begin{aligned}&G^{\mathrm{atom}}_{\alpha\alpha'}(\mathrm{i}\omega) \\ &= \sum_{\Gamma\Gamma'} \frac{(F^{\alpha})_{\Gamma\Gamma'}(F^{\alpha'\dagger})_{\Gamma'\Gamma}(X_\Gamma + X_{\Gamma'})}{\mathrm{i}\omega - E_{\Gamma'} + E_\Gamma},\end{aligned} \tag{30}$$

where $|\Gamma\rangle$ and $|\Gamma'\rangle$ are the atomic eigenstates obtained by exact diagonalization of a single atom problem,

$X_{\Gamma'} = \mathrm{e}^{-\beta E_{\Gamma'}}/(\sum_{\Gamma} \mathrm{e}^{-\beta E_{\Gamma}})$ represents the occupation probability of the local configuration $|\Gamma\rangle$, and $F^{\alpha}_{\Gamma\Gamma'} = \langle\Gamma|f_{\alpha}|\Gamma'\rangle$.

Hubbard-I approximation is

$$\hat{\Sigma} \approx \hat{\Sigma}^{\mathrm{atom}}. \tag{31}$$

In Ref. [26], Savrasov *et al.* propose that the above self energy can be written by the summation of a set of poles, which greatly simplifies the DMFT calculation, because it is not necessary to handle the full frequency dependence of the Green's function. In Hubbard-I approximation, it can be proved that both the atomic Green's function and the self energy are diagonal and can be written in the form of pole expansion if the following two necessary conditions are satisfied. 1) The single particle basis used here should be the one which diagonalize the local density matrix; 2) the atomic Hamiltonian only contains the two-body interaction terms. Obviously, by chosing a proper single particle basis, the atomic Hamiltonian Eq. (19) in general will satisfy the above two conditions and thus can be always written in terms of pole expansion. Unlike Ref. [26], where they only use a few poles to capture the main features of the self energy, in the present implementation, we keep all the poles in the self energy, which makes it more accurate. From Eq. (30), it is very clear that the atomic Green's function has already been expressed in terms of poles and the pole expansion of the corresponding self energy can be obtained using Eq. (29), which will be introduced in details in Appendix A. Therefore, in general the above atomic self energy can be written as

$$\hat{\Sigma}(\mathrm{i}\omega) = \hat{\Sigma}(\infty) + \sum_{i=1}^{n_{\mathrm{p}}} \hat{V}_i^{\dagger}(\mathrm{i}\omega - p_i)^{-1}\hat{V}_i, \tag{32}$$

where i labels the number of poles, n_{p} is the total number of poles in the self energy, and $\hat{V}_i$ is a vector defined in the orbital space describing the distribution of the ith "pole states" among the local orbitals.

3.3. Correction of the density matrices and pole expansion of the self-energy

Once we obtain the converged local self-energy, we reach the point where we correct the $\boldsymbol{k}$-dependent lattice Green's functions as well as the density matrices. In general, we need to do the summation over the Matsubara frequencies, which is time-consuming because realistic materials contain many bands. However, it can be greatly simplified when the self energy can be expressed as the summation of poles, which can be written as

$$\begin{aligned}&\langle\varphi_{n_1\boldsymbol{k}}|\hat{\rho}_{\mathrm{LDA+DMFT}}|\varphi_{n_2\boldsymbol{k}}\rangle\\ &= \frac{1}{\beta}\sum_{\mathrm{i}\omega_n}\langle\varphi_{n_1\boldsymbol{k}}|\\ &\quad\times\frac{1}{\mathrm{i}\omega_n + \mu - \hat{H}_{\mathrm{LDA}} + \hat{V}_{\mathrm{DC}} - \hat{\Sigma}(\mathrm{i}\omega_n)}|\varphi_{n_2\boldsymbol{k}}\rangle.\end{aligned} \tag{33}$$

As pointed out firstly in Ref. [26], when the self energy can be written in terms of poles, the full Green's function can be expressed as the "physical" part of an enlarged "pseudo Hamiltonian", defined as

$$\begin{aligned}&\hat{H}_{\mathrm{ps}}(\boldsymbol{k})\\ &= \begin{pmatrix}\hat{H}_{\mathrm{LDA}}(\boldsymbol{k}) - \hat{V}_{\mathrm{DC}} + \hat{\Sigma}(\infty) & -\hat{V}^{\dagger}\\ -\hat{V} & \hat{P}\end{pmatrix},\end{aligned} \tag{34}$$

where $\hat{H}_{\mathrm{LDA}}(\boldsymbol{k}) = E_{n\boldsymbol{k}}\hat{c}^{\dagger}_{n\boldsymbol{k}}\hat{c}_{n\boldsymbol{k}}$ is the physical Hilbert space, $\hat{V}_i$ is defined in Eq. (32) and $\hat{P} = \mathrm{Diag}(p_1, p_2, \ldots, p_{n_p})$. Therefore, the physical Green's function can be expressed in terms of the eigenstate of the pseudo Hamiltonian simply as

$$\begin{aligned}&\langle\varphi_{n_1\boldsymbol{k}}\left|\frac{1}{\mathrm{i}\omega_n - \hat{H}_{\mathrm{LDA}}(\boldsymbol{k}) + \hat{V}_{\mathrm{DC}} - \hat{\Sigma}(\mathrm{i}\omega_n)}\right|\varphi_{n_2\boldsymbol{k}}\rangle\\ &= \langle\varphi_{n_1\boldsymbol{k}}|\psi^{\mathrm{ps}}_{l\boldsymbol{k}}\rangle\frac{1}{\mathrm{i}\omega_n - E^{\mathrm{ps}}_l(\boldsymbol{k})}\langle\psi^{\mathrm{ps}}_{l\boldsymbol{k}}|\varphi_{n_2\boldsymbol{k}}\rangle,\end{aligned} \tag{35}$$

where $|\psi^{\mathrm{ps}}_{l\boldsymbol{k}}\rangle$ and $E^{\mathrm{ps}}_l(\boldsymbol{k})$ are the eigenstate and eigenvalue of pseudo Hamiltonian, respectively.

Then the sum of frequencies in Eq. (33) can be performed directly as

$$\begin{aligned}&\langle\varphi_{n_1\boldsymbol{k}}|\hat{\rho}_{\mathrm{LDA+DMFT}}|\varphi_{n_2\boldsymbol{k}}\rangle\\ &= \frac{1}{\beta}\sum_{\mathrm{i}\omega_n}\sum_{l\boldsymbol{k}}\langle\varphi_{n_1\boldsymbol{k}}|\psi^{\mathrm{ps}}_{l\boldsymbol{k}}\rangle\frac{1}{\mathrm{i}\omega_n - E^{\mathrm{ps}}_l(\boldsymbol{k})}\langle\psi^{\mathrm{ps}}_{l\boldsymbol{k}}|\varphi_{n_2\boldsymbol{k}}\rangle\\ &= \sum_{l\boldsymbol{k}}\langle\varphi_{n_1\boldsymbol{k}}|\psi^{\mathrm{ps}}_{l\boldsymbol{k}}\rangle\langle\psi^{\mathrm{ps}}_{l\boldsymbol{k}}|\varphi_{n_2\boldsymbol{k}}\rangle n_F[E^{\mathrm{ps}}_l(\boldsymbol{k}) - \mu],\end{aligned} \tag{36}$$

where μ is exactly the chemical potential in Eq. (13), determined by the occupation number of electrons N_{tot} in the unit cell

$$\begin{aligned}N_{\mathrm{tot}} &= \sum_{n\boldsymbol{k}}\langle\varphi_{n\boldsymbol{k}}|\hat{\rho}|\varphi_{n\boldsymbol{k}}\rangle\\ &= \sum_{ln\boldsymbol{k}}|\langle\varphi_{n\boldsymbol{k}}|\psi^{\mathrm{ps}}_{l\boldsymbol{k}}\rangle|^2 n_{\mathrm{F}}[E^{\mathrm{ps}}_l(\boldsymbol{k}) - \mu].\end{aligned} \tag{37}$$

3.4. Evaluation of the real space charge density and completion of the full loop

After DMFT obtains the corrected density matrix $\hat{\rho}$, the real space charge density will be generated based on its Fourier transformation, and then, the new LDA Hamiltonian as well as the new overlap matrices between Bloch states and local orbitals will be recalculated, which closes the full iteration loop for the charge density self consistency. The occupation number of the Bloch basis can also be obtained by

$$n_{\mathrm{LDA+DMFT}} = \sum_{\boldsymbol{k},n_1n_2,\alpha} \langle\alpha_{\boldsymbol{k}}|\varphi_{n_1\boldsymbol{k}}\rangle\langle\varphi_{n_1\boldsymbol{k}}|\hat{\rho}|\varphi_{n_2\boldsymbol{k}}\rangle\langle\varphi_{n_2\boldsymbol{k}}|\alpha_{\boldsymbol{k}}\rangle. \quad (38)$$

3.5. Calculation of physical quantities

3.5.1. Energy functional

Most of the physical quantities we are interested in can be calculated once we have reached the charge density self consistency. First, we present the energy functional of the full loop LDA+DMFT, which can be used to calculate many quantities, such as the total energy and the force. It can be written as[10]

$$E = E_{\mathrm{LDA}}[\rho] - \langle H_{\mathrm{KS}}\rangle_{\mathrm{LDA}} + \langle H_{\mathrm{KS}}\rangle + \langle H_U\rangle - E_{\mathrm{DC}}, \quad (39)$$

where $E_{\mathrm{LDA}}[\rho]$ is the expression of the energy within density-functional theory; $\langle H_{\mathrm{KS}}\rangle_{\mathrm{LDA}} = \mathrm{tr}[\hat{H}_{\mathrm{LDA}}\hat{G}_{\mathrm{LDA}}]$ is the non-interacting energy at LDA level; $\langle H_{\mathrm{KS}}\rangle = \mathrm{tr}[\hat{H}_{\mathrm{LDA}}\hat{G}]$ is the non-interacting energy at DMFT level; $\langle H_U\rangle = \mathrm{tr}[\hat{\Sigma}\hat{G}]/2$ is the interaction energy caused by local correlation interactions; the last term E_{DC} is the double counting energy given in Eq. (23). In the above the meaning for "trace" is defined as

$$\mathrm{tr}[\mathcal{A}] = \frac{1}{\beta}\sum_{n\boldsymbol{k}}\sum_{\mathrm{i}\omega_n}\langle\varphi_{n\boldsymbol{k}}|\mathcal{A}(\mathrm{i}\omega_n)|\varphi_{n\boldsymbol{k}}\rangle, \quad (40)$$

and the integral path surrounds all the energies of the occupied states.

The first and the second term is easily calculated in the LDA framework, and the three terms remaining must be evaluated in the DMFT process, explicitly

$$\langle H_{\mathrm{KS}}\rangle = \sum_{n\boldsymbol{k}} E_{n\boldsymbol{k}}\langle\varphi_{n\boldsymbol{k}}|\hat{\rho}|\varphi_{n\boldsymbol{k}}\rangle, \quad (41)$$

and

$$\begin{aligned}\langle H_U\rangle &= \frac{1}{2}\mathrm{tr}[\hat{\Sigma}\hat{G}] \\ &= \frac{1}{2}\mathrm{tr}[(\hat{G}_0^{-1} - \hat{G}^{-1})\hat{G}] \\ &= \frac{1}{2}\Big[\sum_{m,n\boldsymbol{k}}(E^{\mathrm{ps}}_{m\boldsymbol{k}} - \mu)|\langle\varphi_{n\boldsymbol{k}}|\psi_{m\boldsymbol{k}}\rangle|^2 n_F(E^{\mathrm{ps}}_{m\boldsymbol{k}} - \mu) \\ &\quad -\langle H_{\mathrm{KS}}\rangle + \langle\hat{V}_{\mathrm{DC}}\rangle\Big], \end{aligned} \quad (42)$$

where $\langle H_{\mathrm{KS}}\rangle$ is expressed in Eq. (41), and $\langle\hat{V}_{\mathrm{DC}}\rangle$ is the expected value of $\hat{V}_{\mathrm{DC}}$ at DMFT level

$$\begin{aligned}\langle\hat{V}_{\mathrm{DC}}\rangle &= \sum_i \bar{U}_i\left(n^i_{\mathrm{LDA+DMFT}} - \frac{1}{2}\right)\sum_\alpha\langle\hat{n}^i_\alpha\rangle \\ &= \bar{U}_i\left(n^i_{\mathrm{LDA+DMFT}} - \frac{1}{2}\right)n^i_{\mathrm{LDA+DMFT}}. \end{aligned} \quad (43)$$

Note that here the site index i emerges. We should be very careful in cases where the number of correlated atoms is larger than one. The final expression of the total energy is

$$\begin{aligned}E &= E_{\mathrm{LDA}}[\rho] - \langle H_{\mathrm{KS}}\rangle_{\mathrm{LDA}} + \langle H_{\mathrm{KS}}\rangle \\ &\quad + \frac{1}{2}\Big[\sum_{m,n\boldsymbol{k}}(E^{\mathrm{ps}}_{m\boldsymbol{k}} - \mu)|\langle\varphi_{n\boldsymbol{k}}|\psi_{m\boldsymbol{k}}\rangle|^2 n_{\mathrm{F}}(E^{\mathrm{ps}}_{m\boldsymbol{k}} - \mu) \\ &\quad - \langle H_{\mathrm{KS}}\rangle\Big] + \frac{1}{4}\sum_i \bar{U}_i n^i_{\mathrm{LDA+DMFT}}. \end{aligned} \quad (44)$$

However, if we use Hubbard-I as the impurity solver, and remove the double-counting term by using an integer, the energy functional is given by[11]

$$\begin{aligned}E &= E_{\mathrm{LDA}}[\rho] - \langle H_{\mathrm{KS}}\rangle_{\mathrm{LDA}} + \langle H_{\mathrm{KS}}\rangle \\ &\quad + \frac{1}{2}\Big[\sum_{m,n\boldsymbol{k}}(E^{\mathrm{ps}}_{m\boldsymbol{k}} - \mu)|\langle\varphi_{n\boldsymbol{k}}|\psi_{m\boldsymbol{k}}\rangle|^2 n_{\mathrm{F}}(E^{\mathrm{ps}}_{m\boldsymbol{k}} - \mu) \\ &\quad - \langle H_{\mathrm{KS}}\rangle\Big] + \frac{1}{4}\sum_i \bar{U}_i n^i_0, \end{aligned} \quad (45)$$

where n^i_0 refers to the integer used to remove double counting for the ith correlated atom.

3.5.2. Expressions of DOS and PDOS

In order to calculate the density of state (DOS) or the partial density of state (PDOS) on correlated orbitals, it is necessary to calculate the retarded form of the Green's function. By using the virtue of pole expansion method, we write directly

$$D(\epsilon) = \left(-\frac{1}{\pi}\right)\mathrm{Im}\Big[\sum_{\boldsymbol{k},m,n}\frac{\langle\varphi_{n\boldsymbol{k}}|\psi_{m\boldsymbol{k}}\rangle\langle\psi_{m\boldsymbol{k}}|\varphi_{n\boldsymbol{k}}\rangle}{\epsilon + \mu - E^{\mathrm{ps}}_{m\boldsymbol{k}} + \mathrm{i}\eta}\Big], \quad (\eta \to 0^+), \quad (46)$$

and the PDOS of orbital α

$$D_\alpha(\epsilon) = \left(-\frac{1}{\pi}\right) \mathrm{Im}\left[\sum_{\boldsymbol{k},m} \frac{\langle\alpha_{\boldsymbol{k}}|\psi_{m\boldsymbol{k}}\rangle\langle\psi_{m\boldsymbol{k}}|\alpha_{\boldsymbol{k}}\rangle}{\epsilon+\mu-E^{\mathrm{ps}}_{m\boldsymbol{k}}+\mathrm{i}\eta}\right], \quad (\eta\to 0^+), \tag{47}$$

where

$$\langle\alpha_{\boldsymbol{k}}|\psi_{m\boldsymbol{k}}\rangle = \sum_n \langle\alpha_{\boldsymbol{k}}|\varphi_{n\boldsymbol{k}}\rangle\langle\varphi_{n\boldsymbol{k}}|\psi_{m\boldsymbol{k}}\rangle. \tag{48}$$

4. Benchmark

To validate the LDA+DMFT framework based on the pseudo-potentials-planewave package and tge pole expansion of self energy, we benchmark our implementation by applying it to γ-cerium, americium and paramagnetic NiO. These are three typical strongly correlated systems in which the valence electrons are believed to be on the localized side, as reported in previous literatures. We use the Hubbard-I method as an impurity solver, which is good enough to capture the atomic-like features in the Mott insulators, so we expect that these systems can be well described by our method. We would emphasize here that in our implementation we can replace the Hubbard-I solver by any of the solvers as long as the self energy can be written in pole expansion form.

4.1. Cerium

Cerium metal attracts lots of research interest for its isostructural volume-collapse transition from γ phase to α phase. The volume change is about 15% during the transition, which is possibly driven by the entropy change.[27] Normal LDA calculations can not give a correct description of cerium. As show in Table 1, the equillibrium volume of cerium given by LDA calculations is smaller than the experimental volume of α phase. This is due to the fact that in LDA the f-electrons are treated as itinerant and the strong correlation effects among them cannot be well captured. When an f-electron is treated as a core electron, we see that the equilibrium volume is larger but close to the γ phase. These simple LDA results implies that in γ phase, the f-electrons are more localized than in the α-phase. Therefore, f-electrons in the γ phase are quite close to the localized picture like the situation in Mott insulators, which makes it suitable to apply the Hubbard-I solver. The α-Ce, which is stable in low temperature, is a correlated metal. This is confirmed by many other LDA+DMFT calculations,[27] and also by our newly developed LDA+Gutzwiller method.[28]

In our calculation, for γ-Ce, we used an ultrasoft pseudo-potentional in which 4f, 5s, 5d, 6s orbitals are taken as valence orbitals. The energy cutoff for plane-wave expansion is 12.5 Ha for convergence. Calculations are performed with $10\times10\times10$ $\boldsymbol{k}$-points. For DMFT calculation, the on-site Coulomb interaction U is chosen to be 6.0 eV, as suggested in previous reports.[27,29,30]

Table 1. Lattice parameter and bulk modulus of γ-cerium according to both experiment and calculations.

	Volume/Å^3	Bulk modulus/GPa
Experiments	34.35[31]	21[32]
LDA	22.36	62.09
LDA(fcore)[33]	36.39	30.2
LDA+U/PAW[34]	32.0	34
LDA+DMFT[10]	30.10	48.49
LDA+DMFT	33.29	38.27

The total energy versus volume for γ-cerium obtained by LDA, LDA+U and LDA+DMFT are plotted in Fig. 2. The equilibrium volume and bulk modulus are also shown in Table 1. We can find in Fig. 2 that the equilibrium volume obtained by our LDA+DMFT calculation is very close to the experimental data, which shows great improvements over LDA . The bulk modulus is also improved but still larger than the experimental data, which may imply that the contribution of lattice vibration is inneglectable, as discussed in Ref. [10].

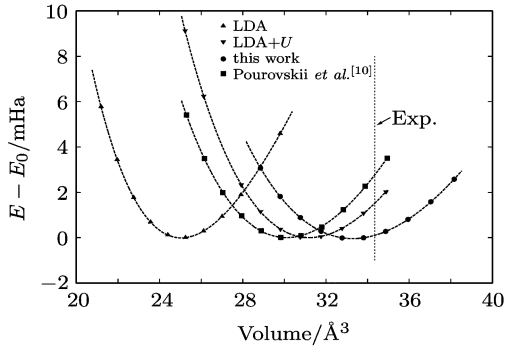


Fig. 2. Total energy versus volume curves obtained by LDA, LDA+U,[10] and LDA+DMFT. The dashed lines are fitted by the Birch EOS. The energy are shifted for different curves. The experimental equilibrium volume is from Ref. [31]. 1 Ha=27.2113845 eV.

Figure 3 shows the 4f PDOS for γ cerium at the equilibrium volume, the position of the two Hubbard bands agree well with the experimental result.

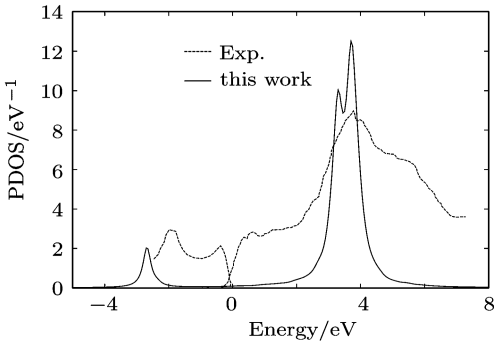


Fig. 3. The 4f PDOS for γ cerium in LDA+DMFT (Hubbard I). XPS and BIS experimental data are from Refs. [35] and [36].

4.2. Americium

Americium (Am), which is widely used in smoke detectors, can be viewed as the "changing point" of the actinide series, where the 5f electrons change from delocalized to localized states.[37] The valence-band ultraviolet photoemission experiment by Naegele *et al.*[38] shows that the 5f states are strongly localized. Am undergoes a series of structure phase transitions with the increment of pressure, from double hexagonal close packed (dhcp, $P6_3/mmc$), to face-centered cubic(fcc, $Fm3m$, 6.1 GPa), face-centered orthorhombic ($Fddd$, 10.0 GPa), and to a primitive orthorhombic structure ($Pnma$, 16 PGa).[39] Therefore, Am provides an interesting playing field in which to investigate the relation between f-electron localization and structural transition. Here, we focus on the fcc phase and dhcp phase.

In the calculation, we used an ultrasoft pseudopotentional containing 5f, 6p, 6d, 7s orbitals as valence orbitals, with the plane-wave expansion kinetic energy cutoff of 12.5 Ha. The LDA self-consistent calculations were performed with $10 \times 10 \times 10$ $\boldsymbol{k}$-points grid for fcc phase, $9 \times 9 \times 3$ $\boldsymbol{k}$-points grid for dhcp phase. For the volume calculation, we only considered density density interaction, and on-site Coulomb interaction $F^{(0)} = 4.5$ eV, for the PDOS calculation, we considered general interaction, and take the atomic values $F^{(2)} = 7.2$ eV, $F^{(4)} = 4.8$ eV, $F^{(6)} = 3.6$ eV.[40]

We present the optimized volume and bulk modulus for both dhcp and fcc phases in Table 2 and Fig. 4. Our LDA+DMFT results are quite close to the experimental data and show great improvement over LDA. In addtion, our results are quite consistent with the results of Ref. [26], in which the full potential LMTO methods are used in the LDA part. The equation of state of Am obtained by our LDA+DMFT calculation is plotted in Fig. 5, which again shows very good agreement with both the experimental data and previous LDA+DMFT calculation based on LMTO method.[26]

Table 2. Am equilibrium volumes and bulk moduli for dhcp and fcc phases by different methods, together with the experimental results.[39,41]

	Volume/Å^3	Bulk modulus/GPa
experiment	29.250	29.9
GGA (dhcp)[42]	19.916	70.0
LDA (dhcp)	18.55	118.99
LDA (fcc)	17.73	169.40
LDA+DMFT (dhcp)	27.04	52.70
LDA+DMFT (fcc)	26.99	50.75
LDA+DMFT[26]	27.4	45

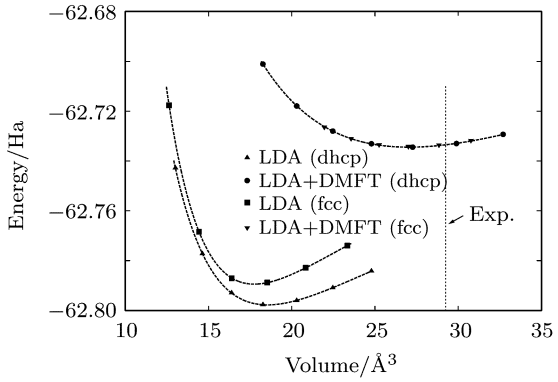


Fig. 4. Total energy per atom of Am obtained by LDA and LDA+DMFT. The LDA+DMFT results of Am for both phases are very close, and the experimental equilibrium volume is denoted by the dotted line.

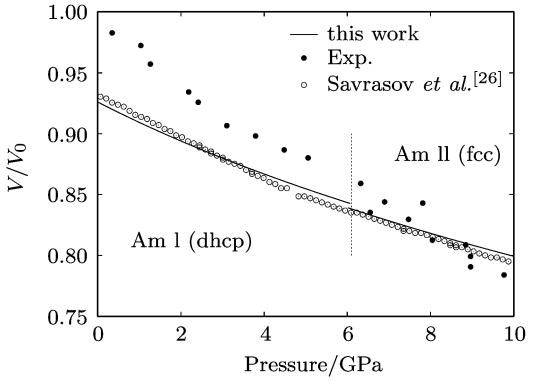


Fig. 5. Calculated P–V relation of dhcp and fcc Am. Here, V_0 is the experimental equilibrium volume, The experimental P–V results[41] are shown by black dots.

Figure 6 shows the 5f partial DOS of fcc phase Am obtained both by our LDA+DMFT calculation and LDA+DMFT(OCA) by Savrasov,[26] together with

the photoemission data from Ref. [38]. Our results are quite consistent with previous calculations and experimental results.

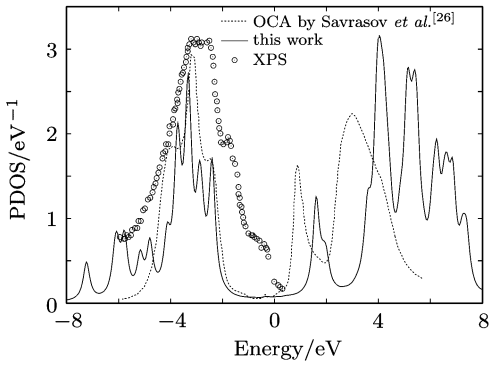


Fig. 6. The spectral function of Am evaluated by LDA+DMFT. The experimental photoemission results from Ref. [38] are denoted by solid dots.

4.3. Paramagnetic phase of NiO

NiO has been heavily studied as a prototype of Mott insulators. It has been studied within the framework of LDA+DMFT by many groups.[43,44] Therefore, NiO can be used as a good benchmark material for the implementation of LDA+DMFT. In this paper, we apply our code to study the paramagnetic phase of NiO. First we plot the PDOS obtained by LDA in Fig. 7, which clearly shows metallic behavior and is not consistent with the experiments. In our LDA+DMFT (Hub1) calculation, we use the Wannier functions as the local basis and choose on-site interaction $U = 8.0$ eV, Hund's coupling $J = 1.0$ eV. The Mott insulating features of NiO then can be well captured by our LDA+DMFT method, as shown by the PDOS in Fig. 8.

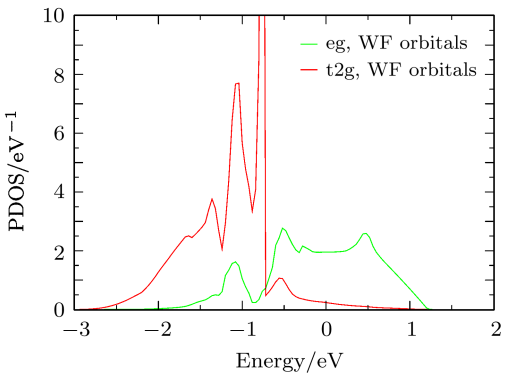


Fig. 7. (colour online) PDOS of NiO obtained by LDA. The main contribution to the Fermi surface is attributed to eg-like Wannier orbitals, and the t2g-like orbitals are almost fully occupied.

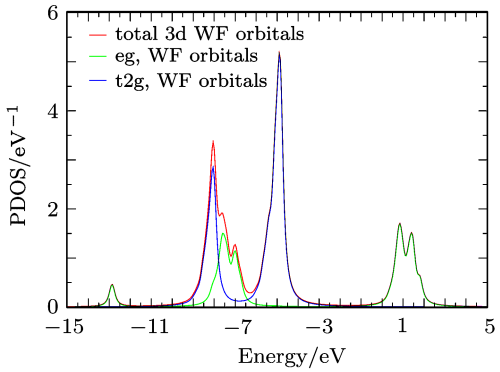


Fig. 8. (colour online) The spectral function of NiO obtained by LDA+DMFT calculation. Compared with LDA results, the t2g-like orbitals are still fully occupied while the eg-like orbitals split into the upper and lower Hubbard bands.

The energy gap obtained by our calculation is around 4.0 eV, which is also quite consistent with the experiments. The photo emission and BIS data obtained by Sawatzky and Allen[45] are also plotted in Fig. 9. We can find that our results fit well with the photo emission and BIS data.

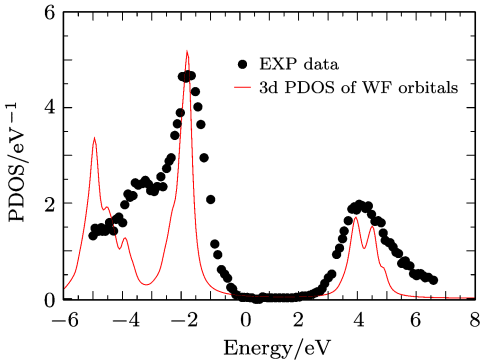


Fig. 9. (colour online) The spectral function of NiO evaluated by LDA+DMFT, in comparison with the experimental data.[45] The behavior of the density of state near the fermi surface fits well with the experimental data.

5. Conclusion

The new implementation of LDA+DMFT based on the pseudo-potential plane-wave method has been introduced in detail in this paper. We choose the Hubbard-I method as the impurity solver to solve the quantum impurity problem generated by DMFT, which is quite suitable for the Mott insulator materials. The most important advantage of the Hubbard-I method is that it is simple, which makes the full loop-charge self-consistent calculation accessible. We also point out that the difficulty of handling the frequency-dependent Green's function can be completely re-

moved by expressing the self energy in terms of pole expansion, which greatly increases the efficiency of the method. Finally, we benchmark our implementation of LDA+DMFT on several important correlation materials including γ-Ce, Am and NiO. Our results for all these materials fit very well with both the experimental data and the previous LDA+DMFT results.

Acknowledgement

The authors thank L. Wang, G. Xu, and F. Lu for their helpful discussion.

Appendix A: Self-energy in pole expansion form

In this appendix, we will introduce how to evaluate self-energy from Green's function in the pole expansion form.

Green's function can be expressed as

$$G(\mathrm{i}\omega) = \sum_{i=1}^{N_\mathrm{G}} \frac{V_i}{\mathrm{i}\omega - P_i}, \tag{A1}$$

where P_i is the ith pole of the Green's function, V_i is the weight of the pole, and N_G is the number of Green's function poles. In addition, the self-energy can be expressed as

$$\Sigma(\mathrm{i}\omega) = \sum_{i=1}^{N_\mathrm{S}} \frac{W_i}{\mathrm{i}\omega - Q_i} + \Sigma(\infty), \tag{A2}$$

where Q_i is the ith pole of the self-energy, W_i is the weight of the pole, and N_S is the number of self-energy poles.

Then the Dyson's equation, Eq. (29), becomes

$$\begin{aligned} &\sum_{i=1}^{N_\mathrm{S}} \frac{W_i}{\mathrm{i}\omega - Q_i} + \Sigma(\infty) \\ &= \mathrm{i}\omega + \mu - \epsilon_\mathrm{imp} - \left[\sum_{i=1}^{N_\mathrm{G}} \frac{V_i}{\mathrm{i}\omega - P_i}\right]^{-1}. \end{aligned} \tag{A3}$$

First, consider the $\Sigma(\infty)$, when $\omega \to \infty$

$$\begin{aligned} &\Sigma(\omega \to \infty) \\ &= \mathrm{i}\omega + \mu - \epsilon_\mathrm{imp} - \left[\sum_{i=1}^{N_\mathrm{G}} \frac{V_i}{\mathrm{i}\omega - P_i}\right]^{-1} \\ &= \mathrm{i}\omega + \mu - \epsilon_\mathrm{imp} - \left[\frac{1}{\mathrm{i}\omega}\sum_{i=1}^{N_\mathrm{G}} \frac{V_i}{1 - \frac{P_i}{\mathrm{i}\omega}}\right]^{-1} \\ &= \mathrm{i}\omega + \mu - \epsilon_\mathrm{imp} - \mathrm{i}\omega \left[\sum_{i=1}^{N_\mathrm{G}} V_i - \frac{1}{\mathrm{i}\omega}\sum_{i=1}^{N_\mathrm{G}} V_i P_i\right]^{-1} \\ &= \mathrm{i}\omega + \mu - \epsilon_\mathrm{imp} - \mathrm{i}\omega \left(1 - \frac{\sum_{i=1}^{N_\mathrm{G}} V_i P_i}{\mathrm{i}\omega}\right) \\ &= \mu - \epsilon_\mathrm{imp} + \sum_{i=1}^{N_\mathrm{G}} V_i P_i. \end{aligned} \tag{A4}$$

For the self-energy poles in Eq. (A3), it corresponds to zero in the square bracket of the right-hand side of Eq. (A3), that is, for $Q \in \{Q_i\}$, we have

$$\sum_{i=1}^{N_\mathrm{G}} \frac{V_i}{Q - P_i} = 0. \tag{A5}$$

The left-hand side is monotonically decreasing between two adjacent Green's function poles, so we could use bisection method to find the self energy poles.

We rewrite Eq. (A3) as

$$\begin{aligned} \sum_{i=1}^{N_\mathrm{s}} \frac{W_i}{\mathrm{i}\omega - Q_i} &= \mathrm{i}\omega + \mu - \epsilon - \Sigma(\infty) \\ &\quad - \left[\sum_{i=1}^{N_g} \frac{V_i}{\mathrm{i}\omega - P_i}\right]^{-1}. \end{aligned} \tag{A6}$$

For the left-hand side

$$\begin{aligned} W_i &= \lim_{\mathrm{i}\omega \to Q_i} \left(\sum_{j=1}^{N_\mathrm{S}} \frac{W_j}{\mathrm{i}\omega - Q_j}\right)(\mathrm{i}\omega - Q_i) \\ &= \lim_{\mathrm{i}\omega \to Q_i} \left[\mathrm{i}\omega + \mu - \epsilon_\mathrm{imp} - \Sigma(\infty) \right. \\ &\quad \left. - \left(\sum_{j=1}^{N_g} \frac{V_j}{\mathrm{i}\omega - P_j}\right)^{-1}\right](\mathrm{i}\omega - Q_i) \\ &= \lim_{\mathrm{i}\omega \to Q_i} -(\mathrm{i}\omega - Q_i)\left(\sum_{j=1}^{N_\mathrm{G}} \frac{V_j}{\mathrm{i}\omega - P_j}\right)^{-1}. \end{aligned} \tag{A7}$$

Here, we define $\delta = \mathrm{i}\omega - Q_i$ and $h(\delta) = \sum_{j=1}^{N_\mathrm{G}} V_j/(Q_i + \delta - P_j)$, expand $h(\delta)$ as

$$h(\delta) \approx \delta \cdot h'(0) = -\sum_{j=1}^{N_\mathrm{G}} \frac{V_j}{(Q_i - P_j)^2} \cdot \delta, \tag{A8}$$

so

$$W_i = \left[\sum_{j=1}^{N_\mathrm{G}} \frac{V_j}{(Q_i - P_j)^2}\right]^{-1}. \tag{A9}$$

Hence, we have obtained both the self-energy pole and its weight.

References

[1] Liu F L, Jiang G, Bai L N and Kong F J 2011 *Acta Phys. Sin.* **60** 037104 (in Chinese)

[2] Qu N R and Gao F M 2011 *Acta Phys. Sin.* **60** 067102 (in Chinese)

[3] Wang X Z, Lin L B, He J and Chen J 2011 *Acta Phys. Sin.* **60** 077104 (in Chinese)

[4] Li X F, Liu Z L, Peng W M and Zhao A K 2011 *Acta Phys. Sin.* **60** 076501 (in Chinese)

[5] Georges A, Kotliar G, Krauth W and Rozenberg M J 1996 *Rev. Mod. Phys.* **68** 13

[6] Lechermann F, Georges A, Poteryaev A, Biermann S, Posternak M, Yamasaki A and Andersen O K 2006 *Phys. Rev.* B **74** 125120

[7] Anisimov V I, Kozhevnikov A V, Korotin M A, Lukoyanov A V and Khafizullin D A 2007 *J. Phys.*: *Condens. Matter* **19** 106206

[8] Savrasov S Y and Kotliar G 2004 *Phys. Rev.* B **69** 245101

[9] Minár J, Chioncel L, Perlov A, Ebert H, Katsnelson M and Lichtenstein A 2005 *Phys. Rev.* B **72** 045125

[10] Pourovskii L V, Amadon B, Biermann S and Georges A 2007 *Phys. Rev.* B **76** 235101

[11] Haule K, Yee C H and Kim K 2010 *Phys. Rev.* B **81** 195107

[12] Andersen O K 1975 *Phys. Rev.* B **12** 3060

[13] Anisimov V I, Aryasetiawan F and Lichtenstein A I 1997 *J. Phys.*: *Condens. Matter* **9** 767

[14] Lichtenstein A I and Katsnelson M I 1998 *Phys. Rev.* B **57** 6884

[15] Savrasov S Y, Kotliar G and Abrahams E 2001 *Nature* **410** 793

[16] Andersen O K and Saha-Dasgupta T 2000 *Phys. Rev.* B **62** R16219

[17] Anisimov V I, Kondakov D E, Kozhevnikov A V, Nekrasov I A, Pchelkina Z V, Allen J W, Mo S K, Kim H D, Metcalf P, Suga S, Sekiyama A, Keller G, Leonov I, Ren X and Vollhardt D 2005 *Phys. Rev.* B **71** 125119

[18] Souza I, Marzari N and Vanderbilt D 2001 *Phys. Rev.* B **65** 035109

[19] Marzari N and Vanderbilt D 1997 *Phys. Rev.* B **56** 12847

[20] Amadon B, Lechermann F, Georges A, Jollet F, Wehling T O and Lichtenstein A I 2008 *Phys. Rev.* B **77** 205112

[21] Trimarchi G, Leonov I, Binggeli N, Korotin Dm and Anisimov V I 2008 *J. Phys.*: *Condens. Matter* **20** 135227

[22] Korotin D M, Kozhevnikov A V, Skornyakov S L, Leonov I, Binggeli N, Anisimov V I and Trimarchi G 2008 Eur. Phys. J. B **98** 91

[23] Vanderbilt D 1996 *Phys. Rev.* B **41** 7892

[24] Hamann D R, Schlüter M and Chiang C 1979 *Phys. Rev. Lett.* **43** 1494

[25] Held K 2007 Advances in Physics **56** 829

[26] Savrasov S Y, Haule K and Kotliar G 2006 *Phys. Rev. Lett.* **96** 036404

[27] Amadon B, Biermann S, Georges A and Aryasetiawan F 2006 *Phys. Rev. Lett.* **96** 066402

[28] Tian M F, Deng X Y, Fang Z and Dai X 2001 *Phys. Rev.* B **84** 205124

[29] Haule K, Oudovenko V, Savrasov S Y and Kotliar G 2005 *Phys. Rev. Lett.* **94** 036401

[30] Amadon B 2011 arXiv:1101.0539

[31] Jeong I K, Darling T W, Graf M J, Proffen Th, Heffner R H, Lee Y, Vogt T and Jorgensen J D 2004 *Phys. Rev. Lett.* **92** 105702

[32] Decremps F, Antonangeli D, Amadon B and Schmerber G 2009 *Phys. Rev.* B **80** 132103

[33] Huang L and Chen C A 2007 *J. Phys.*: *Condens. Matter* 2007 **19** 476206

[34] Amadon B, Jollet F and Torrent M 2008 *Phys. Rev.* B **77** 155104

[35] Wuilloud E, Moser H R, Schneider W D and Baer Y 1983 *Phys. Rev.* B **28** 7354

[36] Wieliczka D, Weaver J H, Lynch D W and Olson C G 1982 *Phys. Rev.* B **26** 7056

[37] Moore K T and van der Laan G 2009 *Rev. Mod. Phys.* **81** 235

[38] Naegele J R, Manes L, Spirlet J C and Müller W 1984 *Phys. Rev. Lett.* **52** 1834

[39] Heathman S, Haire R G, Le Bihan T, Lindbaum A, Litfin K, Méresse Y and Libotte H 2000 *Phys. Rev. Lett.* **85** 2961

[40] Carnall W T and Wybourne B G 1964 *J. Chem. Phys.* **40** 3428

[41] Lindbaum A, Heathman S, Litfin K, Méresse Y, Haire R G, Le Bihan T and Libotte H 2001 *Phys. Rev.* B **63** 214101

[42] Kutepov A and Kutepova S 2004 *J. Magn. Magn. Mater.* **272** E329

[43] Ren X, Leonov I, Keller G, Kollar M, Nekrasov I and Vollhardt D 2006 *Phys. Rev.* B **74** 195114

[44] Kuneš J, Anisimov V I, Lukoyanov A V and Vollhardt D 2007 *Phys. Rev.* B **75** 4

[45] Sawatzky G and Allen J 1984 *Phys. Rev. Lett.* **53** 2339